CORE
Metadata, citation and similar papers at core.ac.uk
Provided by Elsevier - Publisher Connector

International Journal of Solids and Structures 50 (2013) 3097–3105

Contents lists available at SciVerse ScienceDirect

International Journal of Solids and Structures

journal homepage: www.elsevier.com/locate/ijsolstr

Large bending behavior of creased paperboard. II. Structural analysis

Lando Mentrasti [a,*], Ferdinando Cannella [b], Mirko Pupilli [c], Jian S. Dai [d]

[a] Dipartimento di Ingegneria Civile, Edile e Architettura, Facoltà di Ingegneria, Università Politecnica delle Marche, Via Brecce Bianche, 60131 Ancona, Italy
[b] Department of Advanced Robotics, Italian Institute of Technology, Via Morego 30, 16163 Genova, Italy
[c] Dipartimento di Meccanica, Facoltà di Ingegneria, Università Politecnica delle Marche, Via Brecce Bianche, 60131 Ancona, Italy
[d] School of Natural and Mathematical Sciences, King's College London, University of London, Strand, London WC2R 2LS, United Kingdom

ARTICLE INFO

Article history:
Available online 6 June 2013

Keywords:
Creased paperboard
Large bending behavior
Finite rotation kinematics
Large displacement statics
Carton erection

ABSTRACT

The mechanics of a paradigmatic typical carton corner with five creases is analyzed theoretically, in closed form. A general kinematical analysis of the mechanism (in finite rotation) is presented, assuming the versor of the intermediate crease, **s**, as a 2-degree-of-freedom Lagrangian parameter. The rotation θ_c of the cth crease is derived, together with the existence domain and a discussion of the singular configurations.

The actions, driving the carton during a prescribed quasi-static erection program, are derived in a very efficient manner using the Virtual Works Equation, taking into account a *non-linear anholonomic bending constitutive law* of the creased paperboard. In particular, the active and reactive components of the moment ϕ, driving **s** along its path, are identified. No resort to the tangent stiffness computation is required. Some numerical examples illustrate the rotation and the driving forces obtained for both monotone-loading and complex loading–unloading erection paths.

The presented results, "exact" within the scope of the restrictive hypotheses assumed, may be used in a preliminary design approach as well as a benchmark for more realistic FEM or CAE simulators.

© 2013 Elsevier Ltd. All rights reserved.

1. Introduction

The mechanics of the crease creation and its subsequent folding is a formidable structural problem involving a great number of strongly interacting phenomena. Any model predicting the mechanical response of the carton should take into account the following principal elements (Dai and Rees Jones, 1997, 2002; Lu and Akella, 2000; Liu and Dai, 2002; Dai and Cannella, 2008):

Paperboard typology:

- quality of the fibers;
- degree of in-homogeneity and local imperfections;
- number and material of the plies (layers) and their gluing;
- finish coating (possibly different on the "inner" and "outer" side);

Crease typology:

- continuous standard (*normal* in the following) crease;
- partial cut across the thickness, without a pre-crease (*cut* crease);
- discontinuous cut, without a pre-indentation (*dashed cut* crease);
- cut superimposed to a standard crease;

Geometry of the crease formation:

- male die and counter die channel geometry and their wear (round, sharp, ...);
- male/female die material;
- actual depth to paperboard's thickness ratio;
- possible in plane constraints of the paperboard during the crease formation;
- velocity of the crease formation;
- environment moisture and temperature;

Mechanical behavior:

- distinction between the Machine Direction (MD) and the Cross Direction (CD);
- large displacement and strain formulation;
- full 3D anisotropy;
- visco-elastic behavior;
- (pseudo) plastic behavior;
- adhesion/delamination between the plies;
- damage and fracture inside each ply;

* Corresponding author. Tel.: +39 071 2204567; fax: + 39 71 220 4576.
E-mail addresses: mentrasti@univpm.it (L. Mentrasti), ferdinando.cannella@iit.it (F. Cannella), mpupilli@tiscali.it (M. Pupilli), jian.dai@kcl.ac.uk (J.S. Dai).

0020-7683/$ - see front matter © 2013 Elsevier Ltd. All rights reserved.
http://dx.doi.org/10.1016/j.ijsolstr.2013.05.021

Nomenclature

c	index of the cth crease	θ	(signed) crease rotation
dof	degree of freedom	$\dot{\theta}$	rotation derivative with respect to the time
l_c	length of the cth crease	$\dot{\mathbf{q}}$	2-*dof* parameter derivative with respect to the time
$m(\theta, \dot{\theta})$	bending constitutive law: $m = m_L(\theta)$, if $\theta\dot{\theta} > 0$; $m = m_U(\theta)$, if $\theta\dot{\theta} < 0$;	∇_s	gradient with respect to the variable $\mathbf{s}$, $\nabla_s := [\frac{\partial}{\partial s_1} \frac{\partial}{\partial s_2} \mathbf{0}]^T$
		^{T}	(superscript) transpose operator;
$\mathbf{n} \in \Re^3$	normal versor to a facet	$\cdot$	scalar product;
$\mathbf{a}, \mathbf{b}, \mathbf{s} \in \Re^3$	crease versors ($\mathbf{s}$ is the driving versor)	$\times$	vectorial product
$\mathbf{u} \in \Re^3$	is a versor if $\|\|\mathbf{u}\|\| = 1$;	$\otimes$	tensorial product: $\mathbf{u} \otimes \mathbf{vw} := \mathbf{u}\,(\mathbf{v}\cdot\mathbf{w})$
$\mathbf{I}$	tensor identity	$:=$	Ratischauser's symbol of definition
VWE	Virtual Work Equation		
α	facet angle, *cf.* Fig. 2.1b		
δ	variation symbol		

- environment preconditioning: temperature and moisture;
- bending according to the crease or in the opposite direction (Cannella and Dai, 2006; Dai and Cannella, 2008).

Folding/bending processes:

- monotonic load and unload;
- repeated cycles of loading;
- bending velocity;
- environment temperature and moisture.

1.1. The predictive models

The crease formation can be analyzed and simulated as a structure (Dai and Rees Jones, 1998, 2002), with the purpose to predict the macroscopic mechanical behavior of the creased paperboard during folding: Carlsson et al., 1983 – an early particular simple delamination model in very small rotation, Barbier et al., 2005; Cannella and Dai, 2006; Beex and Peerlings, 2009; Giampieri et al., 2011. The geometry, the constitutive equations of each component in the different phases of their mechanical evolution mentioned above, the technological process and the environmental conditions are *assumed to be known* a priori (Ostoja-Starzewski and Stahl, 2000; Ramasubramanian and Wang, 2007; Sato et al., 2008; Suhling et al., 1985; Vannucci, 2010).

However, the results of the experimental investigations, carried out on samples obtained from industrial cartons by Mentrasti et al. (2013), undoubtedly prove that the bending behavior of a creased paperboard under large rotations is heavily dependent on a number of events out of the control of the structural analyzer: the crease depth and the moisture content, primarily.

Therefore, notwithstanding the above mentioned generous works towards a general numerical model to predict the macroscopic bending behavior, the efforts required to obtain a realistic response appear to be prohibitive for a real-time controlled erection of a carton subject to the manufacturing process.

The alternative, proposed in the companion paper mentioned above, is to think to a reconfigurable real-time controlled robot being able to adapt the manipulation process to the carton in production. Nonetheless, the simulation stage requires, among other factors, the consideration of the possible criticalities of the constitutive laws $m(\theta)$. Therefore, the formulation presented below may be used either in a preliminary design approach as well as a benchmark for more realistic FEM or CAE simulators.

2. Kinematics of a paradigmatic carton corner

This central section presents the structural analysis of a paradigmatic example of carton erection. First, a general kinematic analysis in large displacement is derived in closed form. Then the non-linear anholonomic bending constitutive equations of the crease paperboard, presented by Mentrasti et al., 2013, are used in the VWE to derive the driving forces. Owing of the great flexibility of the creased portion of the paperboard with respect to the undamaged remaining part, the out-of-plane displacement of the facets between the creases are considered rigid (this hypothesis can be removed when a significant bending is involved due to the aspect ratio, the position of the actuators or dynamic effects). In the same spirit, a quasi-static loading condition is assumed.

The configuration of a typical carton corner is shown in Fig. 2.1a: the bottom facet f_0 is fixed, while the placement of its adjacent facets f_1, f_2, f_3 and f_4 are defined through the versors $\mathbf{a}$, $\mathbf{b}$, $\mathbf{s} \in \Re^3$ associated with the direct (valley) or inverse (mount) creases, respectively (*cf.* also Fig. 2.3). Their components are not independent because the placement of the versors is restrained by the geometric conditions imposed by the facets, whose amplitude α_i are shown in Fig. 2.1b. In this regards, $\mathbf{s}$ is assumed as the *governing parameter* (Liu and Dai, 2002; Yao and Dai, 2008) of the two independent *dof* mechanism, the configuration singularities being discussed explicitly apart. Each facet, considered to be rigid, imposes of the following constraints (Fig. 2.1b)

$$\mathbf{a} \cdot \mathbf{e}_2 = \cos\hat{\alpha}_1 \tag{1}$$

$$\mathbf{a} \cdot \mathbf{s} = \cos\hat{\alpha}_2 \tag{2}$$

$$\mathbf{b} \cdot \mathbf{s} = \cos\hat{\alpha}_3 \tag{3}$$

$$\mathbf{b} \cdot \mathbf{e}_1 = \cos\hat{\alpha}_4 \tag{4}$$

where $\mathbf{e}_i$ are the versors of the axes (henceforward a hat ^ denotes an assigned quantity). Since the paperboard is assumed to be ini-

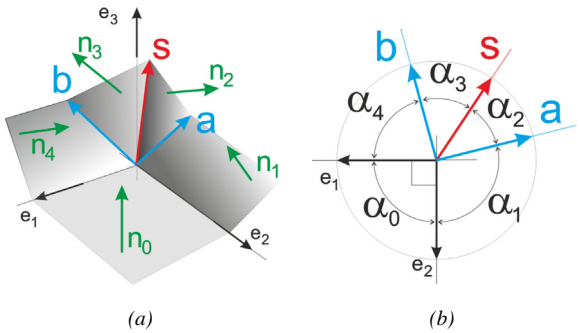

(a) (b)

Fig. 2.1. Versor $\mathbf{a}$, $\mathbf{s}$ and $\mathbf{b}$ describing a typical corner carton (a) and geometrical definition of the angle amplitude α_i, at the initial flat configuration (b). $\mathbf{n}_i$ is the normal of the facet f_i.

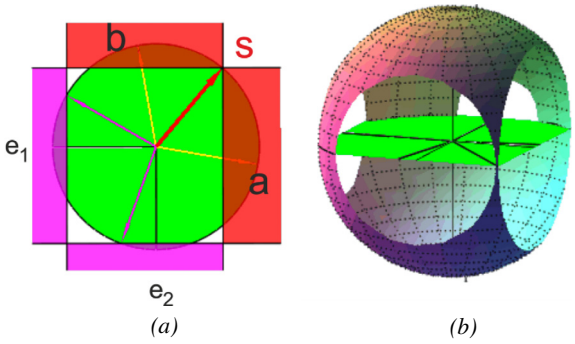

Fig. 2.2. *(a)* The 2D admissible domain for the component $[s_1,s_2]$ *(b)* the entire manifold for the **s** placement.

tially plane $\hat{\alpha}_0+\hat{\alpha}_1+\hat{\alpha}_2+\hat{\alpha}_3+\hat{\alpha}_4=2\pi$ holds ($\hat{\alpha}_0=\pi/2$ is assumed, for simplicity). The *flat origami condition*, namely the Kawasaki-Justin theorem $(\hat{\alpha}_0+\hat{\alpha}_1)-\hat{\alpha}_2+\hat{\alpha}_3-\hat{\alpha}_4=0$ (or similar relationships obtained maintaining inactive a crease different from **a** – *cf.* e.g. (Hull, 2006, Ch. 16)) is usually not satisfied.

2.1. Independent parameters

Equations (1) and (4) state that a_2 and b_2 are known quantities

$$a_2=\mathbf{a}\cdot\mathbf{e}_2\equiv\cos\ \hat{\alpha}_1=:\hat{a}_2 \tag{5}$$

$$b_1=\mathbf{b}\cdot\mathbf{e}_1\equiv\cos\hat{\alpha}_4=:\hat{b}_1 \tag{6}$$

while from Eqs. (2) and (3).

$$s_1a_1+s_3a_3=\cos\hat{\alpha}_2-\hat{a}_2s_2 \tag{7}$$

$$s_2b_2+s_3b_3=\cos\hat{\alpha}_3-\hat{b}_1s_1 \tag{8}$$

results (for the sake of simplicity of notation, the time dependence is omitted).

Since $a_1=\pm\sqrt{1-\hat{a}_2^2-a_3^2}$ and $b_2=\pm\sqrt{1-\hat{b}_1^2-b_3^2}$, the previous equations can be written

$$\pm s_1\sqrt{1-\hat{a}_2^2-a_3^2}+s_3a_3=\cos\hat{\alpha}_2-\hat{a}_2s_2 \tag{9}$$

$$\pm s_2\sqrt{1-\hat{b}_1^2-b_3^2}+s_3b_3=\cos\hat{\alpha}_3-\hat{b}_1s_1 \tag{10}$$

allowing to derive $\{a_3,b_3\}$, and therefore **a** and **b**, as a function of the versor of the intermediate crease, **s**. In fact, squaring Eq. (2) the following equation in a_3 is obtained

$$(a_3)^2(s_1^2+s_3^2)-2s_3(\cos\hat{\alpha}_2-\hat{a}_2s_2)a_3+[(\cos\hat{\alpha}_2-\hat{a}_2s_2)^2-s_1^2(1-a_2^2)]=0 \tag{11}$$

from which

$$a_3=\frac{+s_3(\cos\hat{\alpha}_2-\hat{a}_2s_2)\pm s_1\sqrt{(s_1^2+s_3^2)(1-\hat{a}_2^2)-(\cos\hat{\alpha}_2-\hat{a}_2s_2)^2}}{s_1^2+s_3^2} \tag{12}$$

is derived, when $s_1^2+s_3^2\neq 0$.

The sign ambiguity in the above relationships governs alternative placement of **a** with respect to **s** and $\mathbf{e}_2$ and must be discussed in detail.

(a) $s_1\neq 0$

(a.1) The two solutions for a_3 are both admissible (*cf.* Fig. A.1, representing a quasi-critical configuration: an alternative, $a_1<0$, is possible) and the choice is resolved taking into account the continuity of the evolution process.

(a.2) The remaining component, a_1, can be derived from Eq. (7) as

$$a_1=(\cos\hat{\alpha}_2-\hat{a}_2s_2-s_3a_3)/s_1 \tag{13}$$

(b) $s_1=0$

(b.1) If $s_3\neq 0$ Eq. (5) gives only one solution

$$a_3=(\cos\hat{\alpha}_2-\hat{a}_2s_2)/s_3 \tag{14}$$

and the placement of a is governed by the alternative

$$a_1=\pm\sqrt{1-\hat{a}_2^2-a_3^2} \tag{15}$$

(b.2) Finally, when also $s_3=0$ (see Fig. A.1), two possible fixed singular configurations can be attained provided that $s_2=+1$ or $s_2=-1$ belongs to the domain of definition of **s** (as discussed in the following section). The details are reported in Appendix A and are interesting only as limit cases.

The **b** components are derived in a similar manner. When $s_2^2+s_3^2\neq 0$, from Eq. (10)

$$b_3=\frac{+s_3(\cos\alpha_3-\hat{b}_1s_1)\pm s_2\sqrt{(s_2^2+s_3^2)(1-\hat{b}_1^2)-(\cos\alpha_3-\hat{b}_1s_1)^2}}{s_2^2+s_3^2} \tag{16}$$

(a.1) When $s_2\neq 0$ the two solution for b_3 are both admissible, corresponding to the alternative placement of **b** with respect to **s** and $\mathbf{e}_1$,

(a.2) and the b_2 component is

$$b_2=(\cos\hat{\alpha}_3-\hat{b}_1s_1-s_3b_3)/s_2 \tag{17}$$

(b.1) If $s_2=0$ and $s_3\neq 0$, Eq. (16) gives only one solution

$$b_3=(\cos\hat{\alpha}_3-\hat{b}_1s_1)/s_3 \tag{18}$$

while the multiplicity of the placement of **b** is given by the two choice

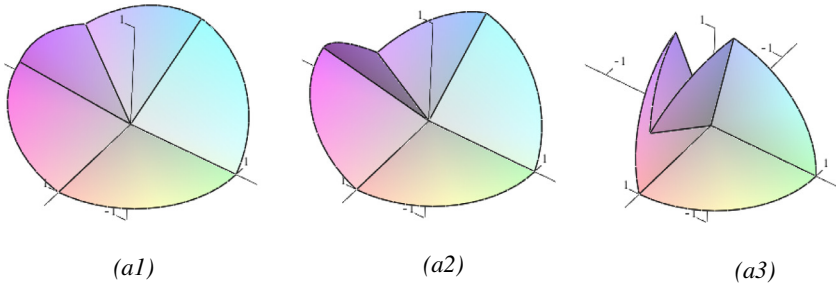

Fig. 2.3. A *linear* erection program starting from the initial flat configuration: *(a)* three intermediate positions.

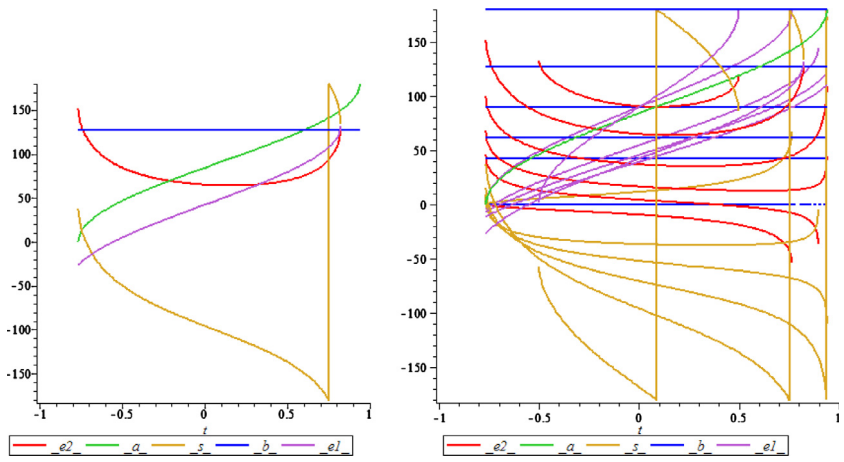

(a) (b)

Fig. 2.4. An erection program with s_1 = constant: *(a)* $s_1 = 0.566$ and *(b)* for several *constant* increasing value of s_1 (abscissa s_2): the vertical jump from −180° to +180° reveals a congruence violation.

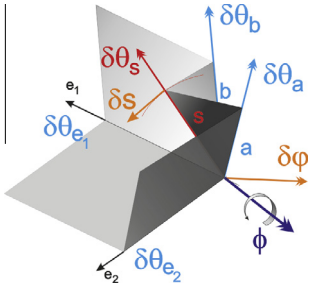

Fig. 2.5. Virtual displacements and rotations δs, $\delta\varphi$, $\delta\theta_c$; driving moment ϕ (axial vectors are represented with a double arrow).

$$b_1 = \pm\sqrt{1-\hat{b}_2^2-\hat{b}_3^2} \tag{19}$$

2.2. Parameters manifold and bidimensional domain of definition

The radicand appearing in Eq. (14) must be non-negative; after a bit of algebra, this condition can be written

$$s_2^2 - 2\hat{a}_2\cos\hat{\alpha}_2 s_2 + \cos^2\hat{\alpha}_2 + \hat{a}_2^2 - 1 \le 0 \tag{20}$$

Since its discriminant, $4(1-\hat{a}_2^2)(1-\cos^2\hat{\alpha}_2) = 4\sin^2\hat{\alpha}_1\sin^2\hat{\alpha}_2$, is always non-negative a real solution for a_3 is possible only when $s_2 \in [\cos(\hat{\alpha}_1+\hat{\alpha}_2), \cos(\hat{\alpha}_1-\hat{\alpha}_2)]$, the extremes being the radices of the quadratic equation. The lower bound (typically negative) corresponds to the starting plane configuration; the upper bound (typically positive) can be interpreted as the placement of **s** for the flat origami closure condition.

A similar conclusion can be drawn for the reality of b_3: $s_1 \in [\cos(\hat{\alpha}_3+\hat{\alpha}_4), \cos(\hat{\alpha}_3-\hat{\alpha}_4)]$, where the endpoints have identical interpretation. Since the trivial constraint $1-s_1^2-s_2^2 \le 0$ must be also satisfied, the admissible domain for the bi-dimensional variable $[s_1,s_2]^T$, becomes the green[1] part shown in Fig. 2.2a.

The entire manifold immersed in 3D, namely the locus of the admissible placements of the versor **s**, is sketched in Fig. 2.2b. It is worth mentioning that at the cusp, $s_3 = 0$, **s** *loses* the meaning of control parameter in favor of the two independent components a_3 and b_3 (*cf.* Appendix A, Section A.2): for these configuration a different *chart* must be chosen.

[1] For interpretation of color in Fig. 2.2, the reader is referred to the web version of this article.

As a final remark, it is important to notice that all these occurrences are only *kinematic* indeterminacy. In fact the variation of the placement of any crease versor involves a variation of some θ_c with a consequent variation of the bending energy of the creases. In the same manner, the infinite energy required to overpass $\theta = \pm 180$ is a natural barrier to prevent some facet compenetrations.

2.3. The relative angles of rotation

Once the normal to the i-th face is defined,

$$n_0 := \mathbf{e}_1 \times \mathbf{e}_2 \equiv \mathbf{e}_3 \tag{21}$$

$$n_1 := (\mathbf{e}_2 \times \mathbf{a})/||\mathbf{e}_2 \times \mathbf{a}|| \tag{22}$$

$$n_2 := (\mathbf{a} \times \mathbf{s})/||\mathbf{a} \times \mathbf{s}|| \tag{23}$$

$$n_3 := (\mathbf{s} \times \mathbf{b})/||\mathbf{s} \times \mathbf{b}|| \tag{24}$$

$$n_4 := (\mathbf{b} \times \mathbf{e}_1)/||\mathbf{b} \times \mathbf{e}_1|| \tag{25}$$

(each denominator is simply $\sin\hat{\alpha}_i$) the current rotation of the crease, $\theta_{\mathbf{c}}$, (namely the relative angle of rotation of the plies adjacent to the crease **c**, assumed to be positive along **c**) can be derived from the following relationships

$$\theta_{\mathbf{e}_2} = \mathbf{a}\tan2(-\mathbf{n}_0 \times \mathbf{n}_1, \mathbf{n}_0 \cdot \mathbf{n}_1) \tag{26}$$

$$\theta_{\mathbf{a}} = \mathbf{a}\tan2(-\mathbf{n}_1 \times \mathbf{n}_2, \mathbf{n}_1 \cdot \mathbf{n}_2) \tag{27}$$

$$\theta_{\mathbf{s}} = \mathbf{a}\tan2(-\mathbf{n}_2 \times \mathbf{n}_3, \mathbf{n}_2 \cdot \mathbf{n}_3) \tag{28}$$

$$\theta_{\mathbf{b}} = \mathbf{a}\tan2(-\mathbf{n}_3 \times \mathbf{n}_4, \mathbf{n}_3 \cdot \mathbf{n}_4) \tag{29}$$

$$\theta_{\mathbf{e}_1} = \mathbf{a}\tan2(-\mathbf{n}_4 \times \mathbf{n}_0, \mathbf{n}_4 \cdot \mathbf{n}_0) \tag{30}$$

where atan2(sin(β), cos(β)) is the function restituting the argument β unambiguously in the interval $[-\pi,+\pi]$;the initial configuration being plane $\theta_c(t=0) \equiv 0$.

The rotations resulting for two erection program of a carton with $\alpha_c = \{90, 80, 60, 50, 80\}$, with c from 0 to 4, are sketched in the following diagrams: a *linear variation* of $[s_1, s_2]^T$ starting from the initial (singular) flat configuration (Fig. 2.3 and Fig. 2.6b) and several cases in which s_1 is maintained constant (Fig. 2.4). It is interesting to note the discontinuity (a jump from −180° to

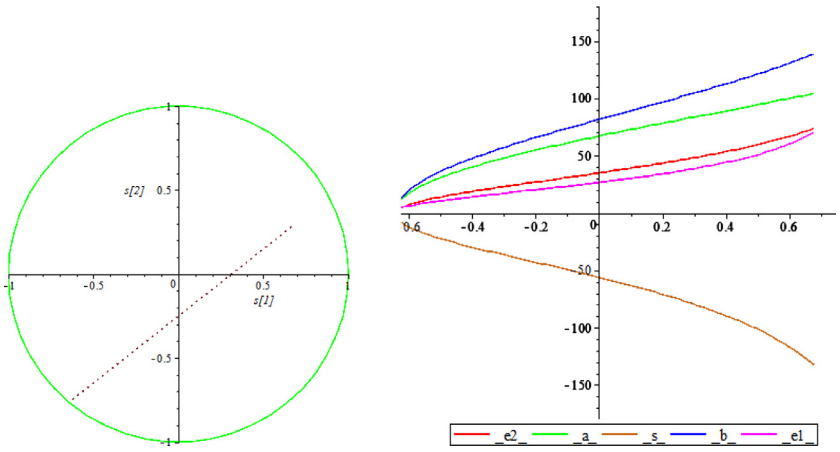

(a) (b)

Fig. 2.6. A *linear* erection path: *(a)* Projection of the trajectory $s[q(t)]$ on the plane $[s_1,s_2]$; *(b)* the rotations θ_c (plotted as function of s_1).

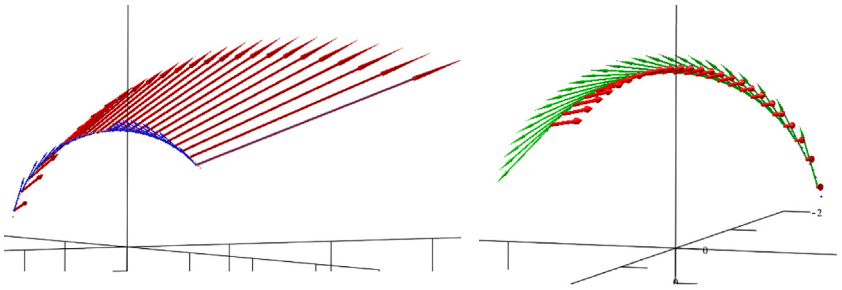

(a) (b)

Fig. 2.7. A *linear* erection path: *(a)* total active (red) and reactive (blue) component of the driving moment. *(b)* the contribution of the crease $\mathbf{e}_1$ alone to the active (red) and reactive component (green) (in this graph the drawing scale is smaller). (For interpretation of the references to color in this figure legend, the reader is referred to the web version of this article.)

+180°) revealing a congruence violation (namely a compenetration of a facet with the adjacent one).

Finally, for the sake of completeness, a non-monotone erection path is shown in Fig. 2.8a, with the consequent non monotone rotation progress shown Fig. 2.9a1–c1.

Remarks

1. The slope of some curve $\theta_c(s_i)$ can become indefinitely large at the extremes of the interval of variation of s_i. This occurrence in no way reflects a geometrical singularity, but it is simply the consequence of choosing a component of the versor **s** as an independent variable: consider, for example, that the variation of s_1 is infinitesimal of the second order, with respect to the rotation of the creases, when the inclination of **s** on the horizontal plane is small.
2. On the other hand this occurrence reveals that a carton cannot be stably erected from the flat configuration by an actuator controlling one of the horizontal component of **s** (*cf.* the last scheme of Fig. 1 in Hicks et al., 2004, or Fig. 15e in Cannella and Dai, 2009).

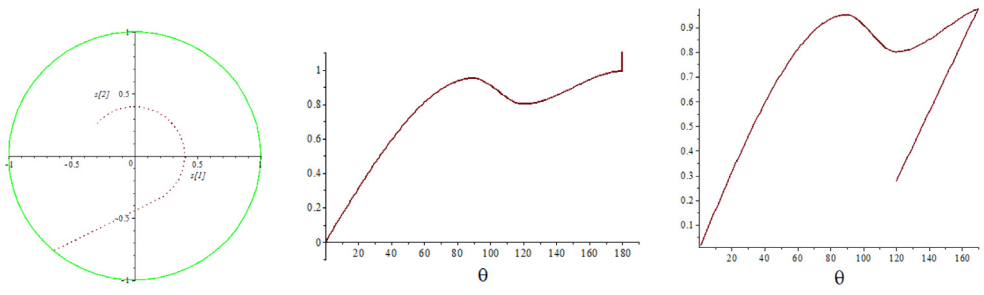

(a) (b) (c)

Fig. 2.8. A *complex* erection path: *(a)* Projection of the trajectory $s[q(t)]$ on the plane $[s_1,s_2]$; *(b)* the loading, $m_L(\theta)$, and *(c)* unloading, $m_U(\theta)$, simplified constitutive equation assumed in these examples.

2.4. The driving forces

The folding of a creased paperboard is a path dependent nonlinear irreversible problem because the constitutive equations $m_c(\theta, \dot{\theta})$ are non-holonomic; furthermore the geometric arrangement of the bodies is so complex that writing down explicitly the equilibrium conditions of each body is very cumbersome.

The efficient alternative to derive the driving forces, actuating a carton erection program, is the VWE $\delta W_{ext} = \delta W_{int}$ (the choice of the kinematic parameters being a matter of practical convenience, as will be shown below).

Since $\mathbf{s}$ has two independent Lagrangian parameters (leaving aside the singular configurations in which the degrees freedom should change), a vector $\mathbf{q} \in \Re^3$ can be defined, containing an appropriate selection of the components of the versors governing the kinematics (e.g. $s_1 = q_1(t)$ and $s_2 = q_2(t)$ is a typical choice; $s_1 \equiv s_2 = q_1(t)$ is the symmetric erection).

Then $\mathbf{a}$, $\mathbf{s}$ and $\mathbf{b}$ are functions of $\mathbf{q}$ and therefore can be written, for each crease c,

$$\theta_c = \theta_c(\mathbf{q}) \tag{31}$$

$$\delta\theta_c = \Theta_c(\mathbf{q})\delta\mathbf{q} \tag{32}$$

$$m_c = m_c(\theta, \dot{\theta}) = m_c(\mathbf{q}, \dot{\mathbf{q}}) \tag{33}$$

(for the sake of brevity, the value and the name of the functions are not distinguished).

By equating the total internal virtual work done by the moments along each crease of length l_c,

$$\delta W_{int} = \Sigma_c l_c m_c(\mathbf{q}, \dot{\mathbf{q}})\delta\theta_c \tag{34}$$

with the external virtual work

$$\delta W_{ext} = Q_1\delta\mathbf{q}_1 + Q_2\delta\mathbf{q}_2 \tag{35}$$

the generalized driving forces Q_1 and Q_2 are finally determined

$$Q_k := \frac{\delta W_{ext}}{\delta q_k} \tag{36}$$

It is interesting to notice the necessary distinction between the actual rotation increment $d\theta_c = \dot{\theta}\, dt$, implicitly appearing in the constitutive equation to detect the loading or unloading behavior, and the virtual arbitrary variation $\delta\theta_c$, generating the virtual work.

2.4.1. Virtual variation of the kinematical parameters

Since the parameter assumed in the geometrical analysis is the *versor* $\mathbf{s}$, then the following results are true (Fig. 2.5):

(i) $\delta\mathbf{s}\cdot\mathbf{s} = 0$; consequently $\delta\mathbf{s}$ can be built in such a way that the orthogonality constraint is identically satisfied as
(ii) $\delta\mathbf{s} := \delta\boldsymbol{\varphi} \times \mathbf{s}$, identifying $\delta\boldsymbol{\varphi} \in \Re^3$ as an arbitrary virtual (infinitesimal) rotation of $\mathbf{s}$. Notice that in this relationship $\delta\mathbf{s}$ is formally express by means of a vector belonging to $\Re^3$; however, it is actually a function of only *two* independent parameters, because the cross-product is a rank-2 linear transformation. On the other hand
(iii) $\delta\boldsymbol{\varphi} := \mathbf{s} \times \delta\mathbf{s}$, is also true when $\delta\mathbf{s}$ is assumed to satisfy $\delta\mathbf{s}\cdot\mathbf{s} = 0$.

Finally, it should be recalled the following elementary

Lemma 1. Let $\mathbf{n} \in \Re^3$ be a versor and $\mathbf{b} \in \Re^3$ arbitrary. The problem *find* $\mathbf{u} \in \Re^3$, *such that* $\mathbf{u} \times \mathbf{n} = \mathrm{b}$, has a (minimal norm) solution $\mathbf{u}_0 := \mathbf{n} \times \mathbf{b}$, if and only if $\mathbf{n}\cdot\mathbf{b} = 0$ (every other solution is $\mathbf{u}_0 + \lambda\,\mathbf{n}$, with $\lambda \in \Re$ arbitrary).

2.4.2. The driving moment (using $\delta\boldsymbol{\varphi}$ as Lagrangian parameter)

Instead of the generalized forces $\mathbf{Q}$, can be more significant to deal with the driving *moment* $\boldsymbol{\phi}$, dual of the rotation angle $\delta\boldsymbol{\varphi}$ of the versor $\mathbf{s}$ (see also the Remark at the end of §3.2). By definition, the external virtual work is simply

$$\delta W_{ext} = \boldsymbol{\phi} \cdot \delta\boldsymbol{\varphi}. \tag{37}$$

By assuming, for the moment, $\delta\mathbf{s}$ as Lagrangian parameter, the virtual rotation of the crease is

$$\delta\theta_c = \frac{\partial\theta_c}{\partial s_1}\delta s_1 + \frac{\partial\theta_c}{\partial s_2}\delta s_2 + 0\delta s_3 = \nabla_s\theta_c \cdot \delta\mathbf{s} \tag{38}$$

where $\nabla_s\,\theta_c := [\frac{\partial\theta_c}{\partial s_1}\ \frac{\partial\theta_c}{\partial s_2}\ 0]^T$, the last component being identically zero because all the kinematic quantities are assumed to be independent of s_3. Using now the change of variable $\delta\mathbf{s} := \delta\boldsymbol{\varphi} \times \mathbf{s}$, $\delta\theta_c$ can be explicitly written as a function of $\delta\boldsymbol{\varphi}$ as

$$\delta\theta_c = \delta\mathbf{s} \cdot \nabla_s\theta_c = \delta\boldsymbol{\varphi} \times \mathbf{s} \cdot \nabla_s\theta_c = \mathbf{s} \times \nabla_s\theta_c \cdot \delta\boldsymbol{\varphi} \tag{39}$$

The VWE, namely $\delta W_{ext} = \delta W_{int}$,

$$\boldsymbol{\phi} \cdot \delta\boldsymbol{\varphi} = \mathbf{s} \times \Sigma_c l_c m_c \nabla_s\theta_c \cdot \delta\boldsymbol{\varphi}, \forall\delta\boldsymbol{\varphi} \tag{40}$$

finally gives the required driving moment

$$\boldsymbol{\phi} = \mathbf{s} \times \Sigma_c l_c m_c(\theta, \dot{\theta})\nabla_s\theta_c \tag{41}$$

owing to the arbitrariness of $\delta\boldsymbol{\varphi}$.

2.4.3. The driving moment (using $\delta\mathbf{s}$ as Lagrangian parameter)

For the sake of completeness, the moment $\boldsymbol{\phi}$ is also derived using the natural variation $\delta\mathbf{s}$, even if the development is a bit involved because in this case $\delta\mathbf{s}$ *is not an arbitrary* vector of $\Re^3$. By writing $\delta\boldsymbol{\varphi} = \mathbf{s} \times \delta\mathbf{s}$, δW_{ext} becomes

$$\delta W_{ext} = \delta\boldsymbol{\varphi} \cdot \boldsymbol{\varphi} = \mathbf{s} \times \delta\mathbf{s} \cdot \boldsymbol{\phi} = \boldsymbol{\phi} \times \mathbf{s} \cdot \delta\mathbf{s}, \tag{42}$$

Using the above expression for $\delta\theta_c = \nabla_s\theta_c\cdot\delta\mathbf{s}$, the VWE gives now

$$[\boldsymbol{\phi} \times \mathbf{s} - \Sigma_c l_c m_c \nabla_s\theta_c] \cdot \delta\mathbf{s} = 0, \quad \forall\delta\mathbf{s} : \mathbf{s} \cdot \delta\mathbf{s} = 0 \tag{43}$$

meaning that the bracketed expression is parallel to $\mathbf{s}$, namely

$$\boldsymbol{\phi} \times \mathbf{s} - \Sigma_c l_c m_c \nabla_s\theta_c = \lambda\mathbf{s}, \lambda \in \Re. \tag{44}$$

The scalar λ can be obtained by multiplying this relationship by $\mathbf{s}$

$$\lambda = -\Sigma_c l_c m_c \nabla_s\theta_c \cdot \mathbf{s}, \tag{45}$$

so that the previous equation becomes

$$\boldsymbol{\phi} \times \mathbf{s} = (I - \mathbf{s} \otimes \mathbf{s})\Sigma_c l_c m_c \nabla_s\theta_c, \tag{46}$$

(the tensorial product, defined as $\mathbf{s} \otimes \mathbf{s}\ \mathbf{v} := \mathbf{s}(\mathbf{s}\cdot\mathbf{v})$, being constant with respect to the crease index).

Since $\mathrm{I} - \mathbf{s} \otimes \mathbf{s}$ is the projector on the plane orthogonal to $\mathbf{s}$, the right hand of Eq. (39) fulfills the necessary compatibility condition to apply the Lemma 1 that gives a solution

$$\boldsymbol{\phi} = \mathbf{s} \times (\boldsymbol{I} - \mathbf{s} \otimes \mathbf{s})\Sigma_c l_c m_c \nabla_s\theta_c, \tag{47}$$

But the operator $\mathbf{s} \times [\mathrm{I} - \mathbf{s} \otimes \mathbf{s}]$ is identical to the operator $\mathbf{s}\times$ so that this solution coincides with the above obtained moment (34).

2.4.4. The driving moment (using $\delta\mathbf{q}$ Lagrangian parameter)

When the Lagrangian parameter is $\delta\mathbf{q}$, the developments is uselessly complicated. The generalized driving forces can be more easily attained from $\boldsymbol{\phi}$ by the *contravariant rule*, $\mathbf{Q}\cdot\delta\mathbf{q} = \boldsymbol{\phi}\cdot\delta\boldsymbol{\varphi}(\delta\mathbf{q})$, $\forall\delta\mathbf{q}$:

$$\begin{aligned}\mathbf{Q} \cdot \delta\mathbf{q} &= \boldsymbol{\phi} \cdot \mathbf{s} \times \delta\mathbf{s} = \boldsymbol{\phi} \cdot \mathbf{s} \times \nabla_{\mathbf{q}}\mathbf{s}\delta\mathbf{q} = (\boldsymbol{\phi} \times \mathbf{s}) \cdot \nabla_{\mathbf{q}}\mathbf{s}\delta\mathbf{q} \\ &= [\nabla_{\mathbf{q}}\mathbf{s}]^{\mathbf{T}}(\boldsymbol{\phi} \times \mathbf{s}) \cdot \delta\mathbf{q}, \forall\delta\mathbf{q}\end{aligned} \tag{48}$$

giving

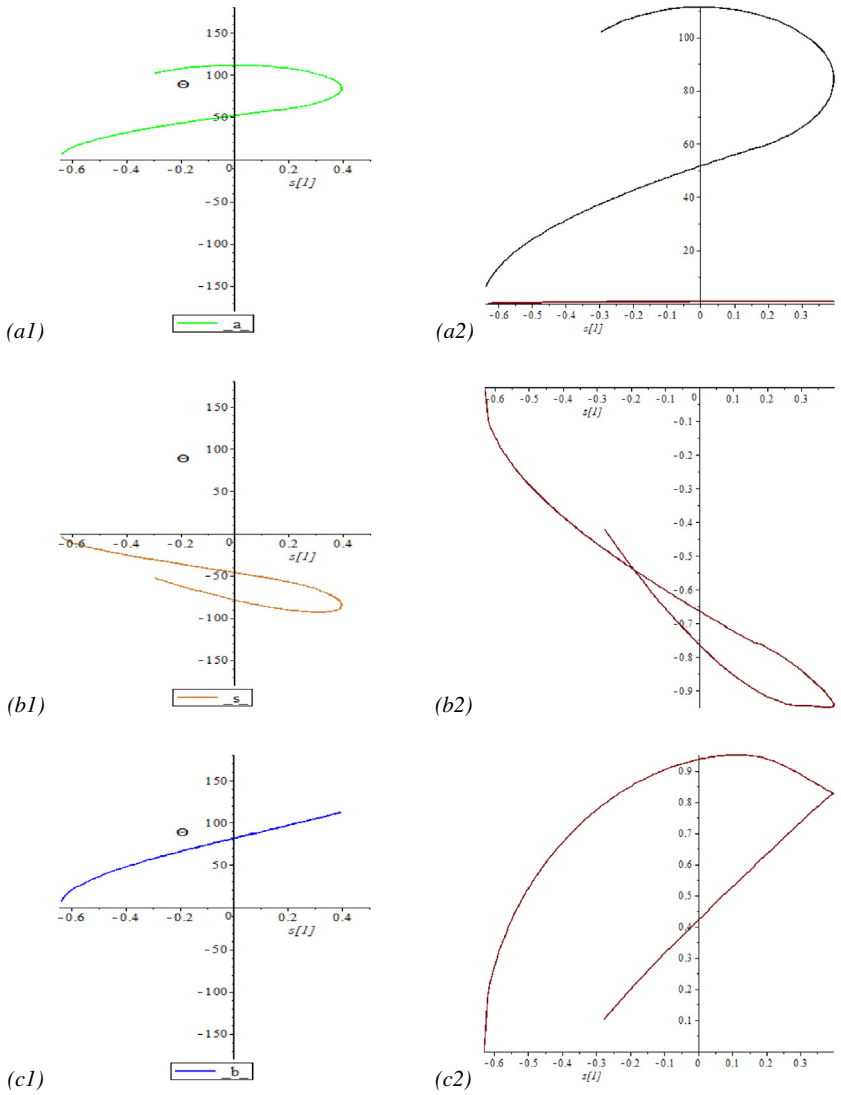

Fig. 2.9. A *complex* erection path: the rotations θ_c and their relevant moment $m_c(\theta,\delta\theta)$ for the creases undergoing a decrease of the rotation after a peak (*a1*, *b1;* in *c1* the downward branch is almost superimposed to the last part of the increasing path). The corresponding moment (*c2*) follows first the loading (unstable) constitutive equation and then the unloading curve shown in Fig. 2.8c.

$$\mathbf{Q} = [\nabla_{\mathbf{q}}\mathbf{s}]^{\mathbf{T}}\boldsymbol{\phi} \times \mathbf{s} \tag{49}$$

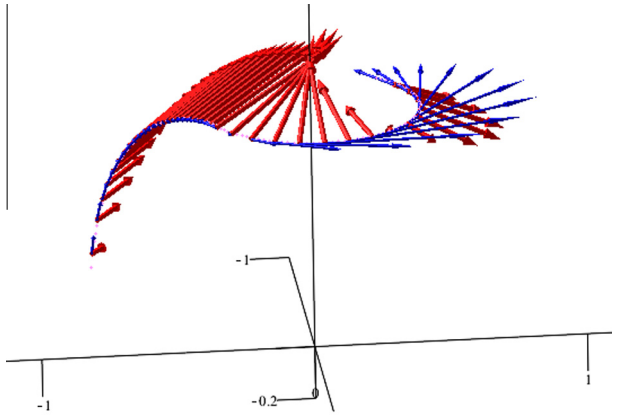

Fig. 2.10. A complex erection path: the active and reactive components of the driving moment on the versor **s**.

2.4.5. The active component $\boldsymbol{\phi}_{d\varphi}$ during the actual erection path

At the current configuration of an actual erection program, the current driving moment can be decomposed in two parts: *(i)* the active component $\boldsymbol{\phi}|_{d\varphi}$, along the actual increment of the rotation $d\boldsymbol{\varphi}$ of the **s** versor; *(ii)* the reactive component orthogonal to $d\boldsymbol{\varphi}$, $\boldsymbol{\phi} - \boldsymbol{\phi}|_{d\varphi}$, doing no (real) work (*cf.* Fig. 2.7 and Fig. 2.10). Notice that $\phi - \boldsymbol{\phi}|_{d\varphi}$ is also orthogonal to **s**, of course.

The scalar component $\boldsymbol{\phi}_{d\varphi}$ of the active driving moment working during an actual erection program can be obtained from the above relationships or simply from the definition of generalized force dual of $d\boldsymbol{\varphi}$ as

$$\phi_{d\phi} = \Sigma_c\, l_c m_c(\theta,\dot{\theta})\frac{d\theta_c}{d\varphi} \tag{50}$$

where $d\varphi = ||\delta\mathbf{s} \times \mathbf{s}||$.

When the versor **s** is not fully controlled, but is actuated assigning only one of its component (e.g. by means of a rotating flap bearing **s**) the problem is more complex: on one hand $d\boldsymbol{\varphi}$ is partially unknown; on the other hand, the component of $\boldsymbol{\phi}$ in the unconstrained direction must be zero (the analytic condition determining the actual path).

Remarks

1. Using $\delta\boldsymbol{\varphi} \in \Re^3$, instead of $\delta\mathbf{q} \in \Re^2$, leads to a very simple derivation of the required 3D-vector $\boldsymbol{\phi}$ (see the following alternative formulation).
2. The obtained expression emphasizes that $\boldsymbol{\phi}$ is always orthogonal to $\mathbf{s}$ (see also Remark 5).
3. Since the component $\boldsymbol{\phi}_\mathbf{s}$ is identically zero, there are only *two* independent components of the driving moment, according to the number of independent Lagrangian parameters.
4. The non-holonomy of the constitutive equations $m_c(\theta_c, \dot{\theta}_c)$ is involved when the loading $(\theta_c\dot{\theta}_c > 0)$ must be distinguished from the unloading $(\theta_c\dot{\theta}_c < 0)$. Therefore the actual value of $\mathrm{d}\theta_c$, evaluated along a real path, must be clearly distinguish from the virtual variation $\delta\theta_c$ that never enter into the final results.
5. Strictly speaking, the above formulation can be regarded as an *Inverse Problem*. One of its remarkable advantages is that the tangent stiffness is not involved at all. In the alternative incremental step-by-step approach, the evaluation of $\frac{dm_c}{d\theta}$ can be a delicate problem from both the experimental and numerical point of view.

2.5. A numerical application

Even though the gradient appearing in $\boldsymbol{\phi}$ can be obtained by a symbolic manipulation of the above kinematic relationships, it is very simpler and more efficient to get it numerically. Typically, when a rotation $\{\theta\}_{i,j}$ is computed on a uniform grid $\{s_1, s_2\}_{i,j}$ then the k-th component of $\nabla_s\,\theta$ can be approximated as follows

$$\left.\frac{\partial\theta}{\partial s_k}\right|_i = \frac{\theta_{i+1} - \theta_{i-1}}{2\Delta s_k} + O(\Delta s^2) \tag{51}$$

The presented formulation is applied to a typical doubly symmetric carton (so that only a quarter is studied), assuming $\alpha_c = \{90, 80, 60, 50, 80\}$ and lengths $l_c = 1$.

2.5.1. Monotone loading path

The carton is subject to the erection *linear path* shown in Fig. 2.6a for which no unloading occurs, since θ_c are monotone functions (Fig. 2.6b).

Fig. 2.7 shows the active and reactive components of the driving moment, according to Remark 4 (the starting point of the path is on the left): the vectors are rooted at the head of each placement of the versor $\mathbf{s}$, along its path.

It is interesting to notice that the contribution to the reactive moment of a single crease can be rather relevant with respect to its active part, as shown in Fig. 2.7b for the crease $\mathbf{e}_1$ alone (for the sake of clarity, now the starting point of the path is on the right). On the contrary, the resulting total reactive driving moment is small because in the studied case the carton is almost symmetric with respect to the erection path in such a way that the opposite addends are almost balanced.

2.5.2. Complex erection path with loading and unloading

The carton is now subject to a complex erection composed by a first path linear, followed by a rotation of the driving versor $\mathbf{s}$ around the vertical axis (its projection is sketched in Fig. 2.8a, while Fig. 2.8b and c show the simplified constitutive behavior assumed in this and in the previous example. Fig. 2.9 shows the rotations θ_c, together with their relevant moment $m_c(\theta, \dot{\theta})$, as a function of one of the current component of versor $\mathbf{s}$. In this path some functions θ_c are non-monotone: therefore, after the peak of θ_c the moment $m_c(\theta, \dot{\theta})$ follows the unloading constitutive equation $m_U(\theta)$.

Finally, the active and reactive components of the moment driving the versor $\mathbf{s}$ along the path are drawn in Fig. 2.10: it is easy to see the *inversion of the sign* of the driving moment revealing the starting point of an **instability branch** of the path.

3. Conclusion

The requirement of increasing the reliability of the reconfigurable robots manipulating origami-type cartons in packaging industry demands an accurate characterization of mechanical behavior of the creased paperboard, with the aim is to point out the possible criticalities of the erection process.

The erection process of typical carton corner with 5 creases is analyzed theoretically in closed form. The finite rotation kinematical analysis of the mechanism is presented, assuming the versor of the intermediate crease, $\mathbf{s}$, as a 2-*dof* Lagrangian parameter.

The rotation θ_c of the c-th crease is derived, together with the existence domain (the manifold containing all the admissible values for $\mathbf{s}$) and a discussion of the singular configurations.

The actions driving the carton during a general prescribed erection program are derived in a very efficient manner using the Virtual Works Equation, completely bypassing the cumbersome explicit equilibrium equations of each facet. It is worthy of pointing out that with this method no resort to the tangent stiffness is required.

Finally, the active and reactive components of the moment $\boldsymbol{\phi}$, driving $\mathbf{s}$ along its path, are identified. Some numerical examples illustrate the obtained results, for both monotone-loading and loading–unloading (unstable branch) erection paths.

Since the presented formulation is an "exact" closed form solution for the erection problem of a typical carton corner (within the scope of the restrictive hypotheses declared above, of course) it may be used as a benchmark for more realistic FEM or CAE simulators.

Appendix A. Singular configurations

If $s_1 = s_3 = 0$ then $s_2 = \pm 1$. The two possibilities lead to qualitatively different configurations and must be discussed separately.

A.1. The case $s_2 = +1$: one dof partial mechanism (Fig. A.1a)

When $s_2 = 1$ the condition (7) gives $0 = \cos\,\hat{\alpha}_2 - \hat{a}_2$, namely $\cos\,\hat{\alpha}_1 = cos\hat{\alpha}_2$, that is

$$\hat{\alpha}_1 = \hat{\alpha}_2 \tag{A.1}$$

this is a **compatibility condition** on the initial data. On the other hand a_3 is undetermined.

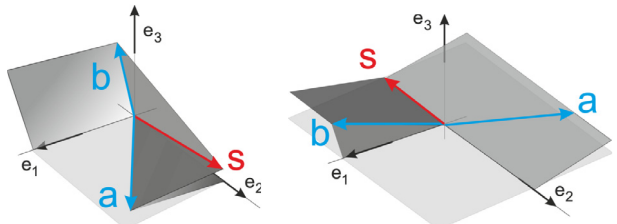

Fig. A.1. *(a)* The singular configuration $s_1 = s_3 = 0$ and a_3 arbitrary. *(b)* The two *dof* singular configuration: $s_1 = s_3 = 0$ and $s_2 = -1$ (while $\theta a \equiv 0$): both a_3 and b_3 can be assumed as Lagrange's parameters.

Similarly, Eq. (8) fixes

$$b_2 = \cos\hat{\alpha}_3 \tag{A.2}$$

consequently a_3 is the unique Lagrange's parameter of the mechanism. The remaining component $b_3 = \pm\sqrt{1-\hat{b}_1^2-\hat{b}_2^2}$ is determined by the continuity condition as discussed above (the evert configuration is not physically attainable).

A.2. The case $s_2 = -1$: 2-dof mechanism (Fig. A.1b)

When $s_2 = -1$ the condition (7) lead to $-\cos\hat{\alpha}_1 = \cos\hat{\alpha}_2$, that is

$$\hat{\alpha}_2 = \pi - \hat{\alpha}_1 \tag{A.3}$$

and, consequently $\hat{\alpha}_3 + \hat{\alpha}_4 = \pi/2$; furthermore $\theta_a \equiv 0$. In this case s cannot control neither a_3 nor b_3 that, as a consequence, becomes the 2-*dof* of the mechanism shown in Fig. A.2 (b_3 being infinitesimal).

Moreover, this singularity always occurs at the initial flat configuration, namely for $s_3 = a_3 = b_3 = 0$. Therefore *if* **s** *is assumed as a control parameter*, in order to have an unambiguous evolution of the carton erection, the process must begin from a configuration in which s_3 and θ_c have small values.

A.3. The rotation about **s** when $\boldsymbol{a} \equiv \boldsymbol{b}$

For the sake of completeness, a final singularity should be mentioned. When $\hat{\alpha}_2 = \hat{\alpha}_3$ is possible that $\mathbf{a} \equiv \mathbf{b}$: in this case **s** can be placed along any generatrix of the cone with axis **b** and angular aperture $\hat{\alpha}_2$.

Appendix B. Supplementary data

Supplementary data associated with this article can be found, in the online version, at http://dx.doi.org/10.1016/j.ijsolstr.2013.05.021.

References

Barbier, C., Larsson, P.-L., Östlund, S., 2005. On dynamic effects at folding of coated papers. Composite Structures 67, 395–402.

Beex, L.A.A., Peerlings, R.H.J., 2009. An experimental and computational study of laminated paperboard creasing and folding. International Journal of Solids and Structures 46, 4192–4207.

Carlsson, L., De Ruvo, A., Fellers, C., 1983. Bending of creased zones of paperboard related to interlaminar defect. Journal of Material Science 18, 1365–1373.

Cannella, F., Dai, J.S., 2006. Crease stiffness and panel compliance of carton folds and their integration in modelling. Journal of Mechanical Engineering Science, Proc IMechE 220 (6), 847–855.

Cannella, F., Dai, J.S., 2009. Origami–Carton tuck-in with a reconfigurable linkage. In: Dai, J.S., Zoppi, M., Kong, X. (Eds.), ASME/IFToMM International Conference on Reconfigurable Mechanisms and Robots, ReMAR 2009, pp. 512–520.

Dai, J.S., Cannella, F., 2008. Stiffness characteristics of carton folds for packaging. Journal of Mechanical Design ASME 130 (2), 1–8.

Dai, J.S., Rees Jones, J., 1997. New configuration model of cartons and their operation. Science and Technology Report PS 97 0066, Unilever Research.

Dai, J.S., Rees Jones, J., 1998. Mobility in metamorphic mechanisms of foldable/erectable kinds. Transactions of ASME: Journal of Mechanical Design 121 (3), 375–382.

Dai, J.S., Rees Jones, J., 2002. Kinematics and mobility analysis of carton folds in packing manipulation based on the mechanism equivalent. Journal of Mechanical Engineering Science, Proc IMechE, Part C 216 (10), 959–970.

Giampieri, A., Perego, U., Borsari, R., 2011. A constitutive model for the mechanical response of the folding of creased paperboard. International Journal of Solids and Structures 48, 2275–2287.

Hull, T., 2006. Project Origami. A.K. Peters, Ltd., Wellesley, MA.

Hicks, B.J., Mullineux, C.B., McPherson, C.J., Medland, A.J., 2004. An energy-based approach for modeling the behavior of a packaging material during processing. Proceedings of the Institution of Mechanical Engineers Part C. Journal of Mechanical Engineering Science 218, 105–118.

Lu, L., Akella, S., 2000. Folding cartons with fixtures: a motion planning approach. IEEE Transaction of Robotics and Automation 16 (4), 346–355.

Liu, H., Dai, J.S., 2002. Carton manipulation analysis using configuration transformation. Proceedings of IMechE, Part C, Journal of Mechanical Engineering Science 216 (5), 543–555.

Mentrasti, L., Cannella, F., Pupilli, M., Dai, S.J., 2013. Large bending behavior of creased paperboard. I. Experimental investigations. International Journal of Solids and Structures, in press, http://dx.doi.org/10.1016/j.ijsolstr.2013.05.018.

Ostoja-Starzewski, M., Stahl, D.C., 2000. Random fiber networks and special elastic orthotropy of paper. Journal of Elasticity 60, 131–149.

Ramasubramanian, M.K., Wang, Y., 2007. A computational micromechanics constitutive model for the unloading behavior of paper. International Journal of Solids and Structures 44, 7615–7632.

Sato, J., Hutchings, I.M., Woodhouse, J., 2008. Determination of the dynamic elastic properties of paper and paperboard from the low-frequency vibration modes of rectangular plates. APPITA Journal 61 (4), 291–296.

Suhling, J.C., Rowlands, R.E., Johnson, M.W., Gunderson, D.E., 1985. Tensorial strength analysis of paperboard. Experimental Mechanics 25 (1), 75–84.

Yao, W., Dai, J.S., 2008. Dexterous manipulation of origami cartons with robotic fingers based on the interactive configuration space. Transactions of the ASME: Journal of Mechanical Design 130 (2), 022303 (8pp.).

Vannucci, P., 2010. On special orthotropy of paper. Journal of Elasticity 99, 75–83.